A low-order decomposition of turbulent channel flow via resolvent analysis and convex optimization

R. Moarref,[1] M. R. Jovanović,[2] J. A. Tropp,[3] A. S. Sharma,[4] and B. J. McKeon[1]

[1]*Graduate Aerospace Laboratories, California Institute of Technology, Pasadena, California 91125, USA*
[2]*Electrical and Computer Engineering, University of Minnesota, Minneapolis, Minnesota 55455, USA*
[3]*Computing and Mathematical Sciences, California Institute of Technology, Pasadena, California 91125, USA*
[4]*Engineering and the Environment, University of Southampton, Southampton, SO17 1BJ, United Kingdom*

We combine resolvent-mode decomposition with techniques from convex optimization to optimally approximate velocity spectra in a turbulent channel. The velocity is expressed as a weighted sum of resolvent modes that are dynamically significant, non-empirical, and scalable with Reynolds number. To optimally represent direct numerical simulations (DNS) data at friction Reynolds number 2003, we determine the weights of resolvent modes as the solution of a convex optimization problem. Using only 12 modes per wall-parallel wavenumber pair and temporal frequency, we obtain close agreement with DNS-spectra, reducing the wall-normal and temporal resolutions used in the simulation by three orders of magnitude. © *2014 AIP Publishing LLC*. [http://dx.doi.org/10.1063/1.4876195]

Wall-bounded turbulent flows are dominated by coherent structures, see, e.g., Smits *et al.*,[1] which motivates the search for their low-order decomposition and modeling. Ideally, a low-order model captures the essential flow physics and is amenable to the techniques that are advanced in systems control and optimization theories. Therefore, it offers several advantages for understanding and controlling wall-turbulence. While a low-order decomposition focuses on capturing the relevant flow quantities such as the velocity fluctuations, a low-order model is concerned with explaining and predicting the flow behavior using the low-order decomposition. Most low-order decompositions are driven by experimental or simulation data and their empirical nature may obscure important flow dynamics.[2–6]

In this paper, we show that a gain-based low-order decomposition that is obtained from the Navier-Stokes equations (NSE) can be used to approximate the turbulent velocity spectra. Recent developments by McKeon and co-workers[7–10] have highlighted the power of this decomposition in capturing several features of wall-turbulence and their Reynolds-number scalings. The proposed decomposition,[7] discussed later, expresses the velocity as a weighted sum of resolvent modes and exhibits two important advantages relative to the other low-order decompositions: (i) The resolvent modes are non-empirical since they represent the most amplified shapes by the linear mechanisms in the NSE; and (ii) The Reynolds-number scaling of the resolvent modes are known.[10] These properties are essential to predicting the behavior of wall-turbulence at high Reynolds numbers. The remaining challenge is related to computation and scaling of the weights that determine the contribution of the resolvent modes to the turbulent kinetic energy and represent the nonlinear interaction of the resolvent modes. Here, we compute the weights such that the resolvent-mode decomposition optimally matches the two-dimensional velocity spectra from direct numerical simulations (DNS) of Hoyas and Jiménez[11] for channel flow with $Re_\tau = 2003$. Even though this yields an empirical
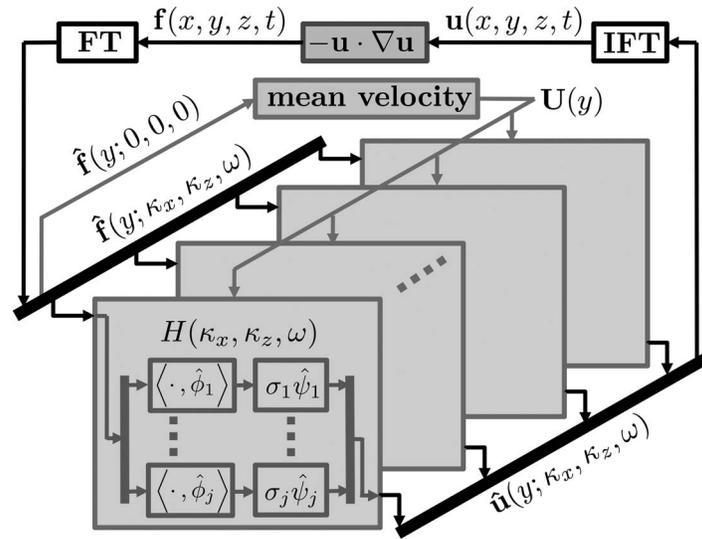
26, 051701-1

FIG. 1. A block-diagram illustrating the linear mechanisms in the NSE and the nonlinear feedback that drives the fluctuations and sustains the mean velocity. FT and IFT stand for Fourier transform and inverse Fourier transform. The resolvent operator H governs the relationship between the nonlinearity $\hat{\mathbf{f}}$ and the fluctuations $\hat{\mathbf{u}}$. The singular value decomposition of H yields an ordered set of most amplified forcing and response modes that are used as a basis for wall-normal decomposition of the fluctuations.

way for computing the weights, theoretical developments for their non-empirical determination is the subject of ongoing research.

Consider the NSE

$$\partial \mathbf{u}/\partial t + (\mathbf{u} \cdot \nabla)\mathbf{u} + \nabla P = (1/Re_\tau)\nabla^2 \mathbf{u}, \nabla \cdot \mathbf{u} = 0, \tag{1}$$

where $\mathbf{u} = [\, u \; v \; w \,]^T$ is the velocity vector in the streamwise x, wall-normal $y \in [0, 2]$, and spanwise z directions, t is time, P is the pressure, and ∇ is the gradient operator. The Reynolds number $Re_\tau = u_\tau h/\nu$ is defined based on the channel half-height h, kinematic viscosity ν, and friction velocity $u_\tau = \sqrt{\tau_w/\rho}$, where τ_w is the shear stress at the wall, and ρ is the density. Velocity is normalized by u_τ, spatial variables by h, time by h/u_τ, pressure by ρu_τ^2, and plus denotes normalization by the viscous scale, e.g., $y^+ = Re_\tau y$. The resolvent-mode decomposition for channel flow is summarized in Eqs. (2) and (3), see also Fig. 1. The Fourier modes are the appropriate basis in the homogeneous wall-parallel directions and time,

$$\mathbf{u}(x, y, z, t) = \iiint_{-\infty}^{\infty} \hat{\mathbf{u}}(y, \kappa_x, \kappa_z, \omega)\, e^{i(\kappa_x x + \kappa_z z - \omega t)} d\kappa_x \, d\kappa_z \, d\omega. \tag{2}$$

Here, the hat denotes the Fourier coefficients, κ_x and κ_z are the streamwise and spanwise wavenumbers, and ω is the temporal frequency. The nonlinear term in (1) is considered as a forcing term $\mathbf{f} = -(\mathbf{u} \cdot \nabla)\mathbf{u}$ that drives the velocity fluctuations around the turbulent mean velocity $\mathbf{U} = [\, U(y) \, 0 \, 0 \,]^T = \hat{\mathbf{u}}(y, 0, 0, 0)$,

$$-i\omega\hat{\mathbf{u}} + (\mathbf{U} \cdot \nabla)\hat{\mathbf{u}} + (\hat{\mathbf{u}} \cdot \nabla)\mathbf{U} + \nabla\hat{p} - (1/Re_\tau)\Delta\hat{\mathbf{u}} = \hat{\mathbf{f}}, \nabla \cdot \hat{\mathbf{u}} = 0,$$

where $\nabla = [\, i\kappa_x \; \partial_y \; i\kappa_z \,]^T$ and $\Delta = \partial_{yy} - \kappa_x^2 - \kappa_z^2$. The input-output relationship between $\hat{\mathbf{f}}$ and $\hat{\mathbf{u}}$ is governed by the resolvent operator H, see Moarref *et al.*[10] for details,

$$\hat{\mathbf{u}}(y, \boldsymbol{\kappa}, \omega) = H(\boldsymbol{\kappa}, \omega)\hat{\mathbf{f}}(y, \boldsymbol{\kappa}, \omega),$$

where $\boldsymbol{\kappa} = [\, \kappa_x \; \kappa_z \,]$ is the wavenumber vector. For any $(\boldsymbol{\kappa}, \omega)$, a complete basis in y is determined using the Schmidt (singular value) decomposition of H. This yields two orthonormal sets of unit-energy forcing modes $\hat{\boldsymbol{\phi}}_j = [\, \hat{f}_{1j} \; \hat{f}_{2j} \; \hat{f}_{3j} \,]^T$ and unit-energy response modes $\hat{\boldsymbol{\psi}}_j = [\, \hat{u}_j \; \hat{v}_j \; \hat{w}_j \,]^T$ (henceforth "resolvent modes") that are ordered by the corresponding gains $\sigma_1 \geq \sigma_2 \geq \cdots > 0$. Each Fourier

coefficient in (2) can be approximated using a weighted sum of the first N resolvent modes

$$\hat{\mathbf{u}}(y, \boldsymbol{\kappa}, \omega) = \sum_{j=1}^{N} \chi_j(\boldsymbol{\kappa}, \omega)\, \sigma_j(\boldsymbol{\kappa}, \omega)\, \hat{\boldsymbol{\psi}}_j(y, \boldsymbol{\kappa}, \omega), \tag{3}$$

where the weights χ_j represent the projection of $\hat{\mathbf{f}}$ onto the first N forcing modes $\hat{\boldsymbol{\phi}}_j$

$$\hat{\mathbf{f}}(y, \boldsymbol{\kappa}, \omega) = \sum_{j=1}^{N} \chi_j(\boldsymbol{\kappa}, \omega)\, \hat{\boldsymbol{\phi}}_j(y, \boldsymbol{\kappa}, \omega), \quad \chi_j(\boldsymbol{\kappa}, \omega) = \int_0^2 \hat{\boldsymbol{\phi}}_j^*(y, \boldsymbol{\kappa}, \omega)\, \hat{\mathbf{f}}(y, \boldsymbol{\kappa}, \omega)\, \mathrm{d}y.$$

Even though the energy of each mode is determined by the product of the corresponding gain and weight, we separately study σ_j and χ_j to distinguish the linear and nonlinear mechanisms in the NSE.

Each resolvent mode represents a propagating wave with streamwise and spanwise wavelengths $\lambda_x = 2\pi/\kappa_x$ and $\lambda_z = 2\pi/\kappa_z$ and streamwise speed $c = \omega/\kappa_x$, as suggested by the Fourier decomposition (2). The resolvent modes are localized around the critical wall-normal location y_c where the mode speed equals the local mean velocity,[7] i.e., $c = U(y_c)$. Moarref *et al.*[10] analytically established that the Reynolds number scalings of the resolvent modes are determined by the mode speed and the different regions of the mean velocity, i.e., the inner- and outer-scaled regions and the logarithmic overlap region in the classical picture.[12] Owing to the integral role of c in the wall-normal localization and scalings of the resolvent modes, the Fourier-transformed variables are parameterized by c instead of ω in the rest of this paper. In addition, we confine our attention to the modes with $0 \le c \le U_{cl}$ where $U_{cl} = U(1)$ denotes the centerline velocity. This conservative choice is motivated by a range of observations, summarized by LeHew *et al.*,[13] that the convective velocity of energetic eddies in turbulent flows is approximately confined between $8u_\tau$ and U_{cl}.

The effectiveness of the resolvent-mode decomposition for representing the turbulent spectra is evaluated by finding the optimal weights that minimize the deviation between the spectra resulting from DNS[11] and from the resolvent-mode decomposition. The premultiplied three-dimensional streamwise energy spectrum is defined as

$$E_{uu}(y, \boldsymbol{\kappa}, c) = \kappa_x^2 \kappa_z\, \hat{u}(y, \boldsymbol{\kappa}, c)\, \hat{u}(y, \boldsymbol{\kappa}, c)^*. \tag{4}$$

The additional power of κ_x in (4) facilitates computation of the time-averaged premultiplied two-dimensional streamwise energy spectrum by integration over c instead of ω

$$E_{uu}(y, \boldsymbol{\kappa}) = \int_0^{U_{cl}} E_{uu}(y, \boldsymbol{\kappa}, c)\, \mathrm{d}c. \tag{5}$$

The contribution of the first N resolvent modes to $E_{uu}(y, \boldsymbol{\kappa}, c)$ is determined by substituting $\hat{u}$ from (3) in (4). Since E_{uu} is a quadratic function of the resolvent weights, selecting χ_j in order to minimize the deviation from the simulation-based spectra results in a non-convex optimization problem. The globally optimal solution of this class of problems is known to be difficult to find. To overcome this challenge, we introduce an $N \times N$ weight matrix $X(\boldsymbol{\kappa}, c)$ whose ijth element is determined by

$$X_{ij}(\boldsymbol{\kappa}, c) = \chi_i^*(\boldsymbol{\kappa}, c)\, \chi_j(\boldsymbol{\kappa}, c), \tag{6}$$

and express E_{uu} as a linear function of X

$$E_{uu}(y, \boldsymbol{\kappa}, c) = \mathrm{Re}\left\{ \mathrm{tr}\big(A_{uu}(y, \boldsymbol{\kappa}, c)\, X(\boldsymbol{\kappa}, c)\big) \right\}. \tag{7}$$

Here, Re is the real part of a complex number, $\mathrm{tr}(\,\cdot\,)$ is the matrix trace, $A_{uu}(y, \boldsymbol{\kappa}, c)$ is the $N \times N$ energy density matrix whose ijth element is determined by the resolvent modes,

$$A_{uu,ij}(y, \boldsymbol{\kappa}, c) = \kappa_x^2 \kappa_z\, \sigma_i(\boldsymbol{\kappa}, c)\, \sigma_j(\boldsymbol{\kappa}, c)\, \hat{u}_i(y, \boldsymbol{\kappa}, c)\, \hat{u}_j(y, \boldsymbol{\kappa}, c)^*. \tag{8}$$

The expressions (5)–(8) for the wall-normal and spanwise energy intensities E_{vv} and E_{ww} and the Reynolds stress E_{uv} are obtained similarly.

For given κ, we formulate the following optimization problem

$$\underset{X,\,e}{\text{minimize}}\ e(\kappa)$$

$$\text{subject to}\ \frac{\left\| E_{r,\text{DNS}}(y,\kappa) - \int_0^{U_{cl}} \text{Re}\left\{ \text{tr}\left(A_r(y,\kappa,c)\, X(\kappa,c) \right) \right\} \mathrm{d}c \right\|^2}{\| E_{r,\text{DNS}}(y,\kappa) \|^2} \ \leq\ e(\kappa) \qquad (9)$$

$$X(\kappa,c) \succeq 0$$

$$\text{rank}\left(X(\kappa,c) \right)\ =\ 1,$$

for the weight matrices $X(\kappa,c)$ and the deviation error $e(\kappa)$. Here, the DNS-based spectra $E_{r,\,\text{DNS}}$ and the energy density matrices A_r, with $r = \{uu, vv, ww, uv\}$, are the problem data (obtained from simulations[11] and the resolvent modes, respectively). The optimization problem (9) is formulated in order to simultaneously minimize the deviation errors for all three velocity spectra and the Reynolds stress co-spectrum. In the first constraint, the integral term quantifies the model-based energy spectrum and is obtained from (5) and (7). The last two constraints follow from the definition of the weight matrix X in (6), and require it to be positive semi-definite and rank-1. The norm $\|g\|^2 = \int_{y^+=5}^{y=1} |g(\ln y^+)|^2 \mathrm{d}\ln y^+$ is defined such that the deviation between the DNS-based and the model-based spectra is equally penalized in the channel core and close to the walls. This norm is different from the standard energy norm (L_2) which is used to compute the resolvent modes. The lower limit $y^+ = 5$ equals the smallest wall-normal location where the DNS data are available.

For any κ, (9) is discretized with N_y logarithmically spaced points between $y^+ = 5$ and $y = 1$ and N_c linearly spaced points between $c = 0$ and U_{cl}. Furthermore, by defining

$$X_l\ =\ X(\kappa, c_l),\ A_{r,lm}\ =\ A_r(y_m, \kappa, c_l),\, l\ =\ \{1, 2, \ldots, N_c\},\, m\ =\ \{1, 2, \ldots, N_y\},$$

we can use (5) and (7) to obtain

$$E_r(y_m, \kappa)\ =\ \sum_{l=1}^{N_c} \text{Re}\left\{ \text{tr}(A_{r,lm}\, X_l) \right\},\, m\ =\ \{1, 2, \ldots, N_y\},\, r\ =\ \{uu, vv, ww, uv\}.$$

The DNS data are interpolated on the wall-parallel wavenumbers and the wall-normal locations that are considered in the minimization problem.

We note that the rank constraint represents the only source of non-convexity in the optimization problem (9). For the special case where $N = 1$, this problem is convex since the rank constraint is eliminated. Even though one resolvent mode per κ and c is sufficient to represent and predict the streamwise energy intensity at high Re_τ,[10] it cannot simultaneously represent the turbulent velocity spectra in the streamwise, wall-normal, and spanwise directions.[14] Therefore, we consider the general case where $N > 1$. The computational challenge is that the optimization problem (9) is not convex for $N > 1$ due to the rank constraint on X_l. In general, there is no guarantee that the globally optimal solution of non-convex problems can be found. However, a rank-1 solution of problem (9) that yields the globally optimal deviation error $e(\kappa)$ can be obtained using the following procedure, see Huang and Palomar[15] for details:

(i)   Remove the rank constraint in (9) and solve the resulting semi-definite programming problem using convex optimization solvers such as CVX.[16] This yields a globally optimal deviation error e and a typically full-rank optimal solution $\{X_l\}_{l=1,2,\ldots,N_c}$.

(ii) While $\sum_{l=1}^{N_c} \text{rank}(X_l)^2 > N_c$, iterate (iii)–(vi).

(iii) Decompose $X_l = V_l V_l^*$ for $l = 1, 2, \ldots, N_c$.

(iv) Find a non-zero Hermitian solution $\{Y_l\}_{l=1,2,\ldots,N_c}$, with the same rank as $\{X_l\}_{l=1,2,\ldots,N_c}$, to the following linear system of equations

$$\sum_{l=1}^{N_c} \text{Re}\left\{ \text{tr}\left(V_l^* A_{r,lm} V_l Y_l \right) \right\}\ =\ 0,\, m\ =\ \{1, 2, \ldots, N_y\},\, r\ =\ \{uu, vv, ww, uv\}.$$

(v)   Let λ be the maximum of the absolute values of the eigenvalues of Y_1 to Y_{N_c}.

(vi) Update $X_l = V_l(I_l - Y_l/\lambda)V_l^*$, where I_l is the identity matrix of the same size as Y_l.

The above procedure begins with the globally optimal solution in the absence of the rank constraint and, at each iteration, computes a new solution with a smaller rank without changing the globally optimal deviation error e. The update law in step (vi) involves two terms: The term $V_l V_l^*$ equals the present weight matrix, cf. step (iii), and the term $V_l(Y_l/\lambda)V_l^*$ lies in the null space of the operator that maps the weight matrix to the energy spectra, cf. step (iv) and Eq. (7). Consequently, the energy spectrum resulting from the updated X_l is the same as the original globally optimal solution, and the deviation error remains unchanged. In addition, since λ is an eigenvalue of Y_l, subtracting $V_l(Y_l/\lambda)V_l^*$ from $V_l V_l^*$ reduces the rank of X_l. Notice that the rank of the globally optimal solution can be reduced as long as the linear system of equations in (iv) has a non-zero solution.[15] This system of equations consists of $4N_y$ equations and $N_c N^2$ unknowns. Therefore, a non-zero solution exists if $4N_y < N_c N^2$. To satisfy this requirement, we choose $N_y = 60$, $N_c = 100$, and $N > 1$. It should be noted that computation of the optimal solution becomes more expensive for larger values of N_y, N_c, and N. This is because a larger N_y results in a larger number of constraints and larger values of N_c and N result in a larger number of unknowns in the problem. In addition, a larger N increases the number of wall-normal grid points that are required to capture the complex shapes of higher-order resolvent modes. Our results show negligible sensitivity to additional increase in N_y and N_c.

Problem (9) is solved using $N = 2$ to 12 resolvent modes per κ and c. The channel symmetry around the center plane results in paired resolvent modes that are symmetric/anti-symmetric counterparts of each other.[10] For each pair of resolvent modes, the mode corresponding to the larger singular value is used. Even though the number of modes that are necessary for representing the spectra may vary for different wavenumber/speed combinations, considering a constant N is sufficient to showcase the main trends. We show that $N = 12$ yields a good agreement between the model-based spectra and the spectra obtained from DNS and that increasing N beyond 12 results in a diminishing return. The convergence analysis of the spectra as N tends to infinity is beyond the scope of the present letter and a subject of ongoing research.

Figure 2 compares the turbulent spectra from DNS[11] (solid contours) and the spectra obtained using $N = 2$ (left column), 6 (center column), and 12 (right column) resolvent modes per κ and c (dotted contours). The contours show 10% to 90% of the maximum in the DNS data with increments of 20%. We see that even 2 resolvent modes are sufficient to capture the general features of the turbulent spectra. The streamwise and spanwise spectra are better matched while the 90% levels in the wall-normal and the uv spectra are not captured.

Using 6 resolvent modes significantly improves matching of the wall-normal and spanwise spectra. The peaks of the streamwise and uv spectra are matched more accurately even though the 90% level in the uv spectrum is still absent. Using 12 resolvent modes results in close matching of the wall-normal and spanwise spectra and emergence of the 90% level in the uv spectrum. Notice that the spectra for small wavelengths ($\lambda_x^+ \lesssim 600$) are well-captured using $N = 12$ while representing the spectra for larger wavelengths requires more resolvent modes. The deviation error for the inner-scaled peak ($\lambda_x^+ = 700$, $\lambda_z^+ = 100$) and the outer-scaled peak ($\kappa_x = 0.6$, $\kappa_z = 6$) of the streamwise spectrum is respectively 22% and 62% using $N = 12$ resolvent modes. Figure 3 shows the energy intensities and the Reynolds stress obtained from DNS[11] (black curves) and $N = 2$ to 12 optimally weighted resolvent modes per κ and c (colored curves). The arrows show the direction of increasing N. For $N = 12$, the deviation errors in the streamwise, wall-normal, and spanwise intensities and the Reynolds stress are, respectively, 20%, 17%, 6%, and 25%.

The present work shows that a small number of resolvent modes ($NN_c = 12 \times 100$) per wall-parallel wavenumber pair can simultaneously approximate the turbulent velocity spectra and the Reynolds stress co-spectrum in a turbulent channel. This number is less than 0.03% of the number of degrees of freedom in DNS[11] (663×7730, where 633 and 7730 are, respectively, the number of wall-normal points and the number of temporal fields that are averaged to obtain the spectra). The actual reduction in the number of degrees of freedom is even larger since the optimal solution is sparse in the mode speed; for example, the weights corresponding to approximately 60% and 80% of the resolvent modes are zero for the inner- and outer-scaled peaks of the streamwise spectrum, respectively. In addition, we highlight that the resolvent-mode decomposition exhibits several important properties that are essential to predicting the behavior of
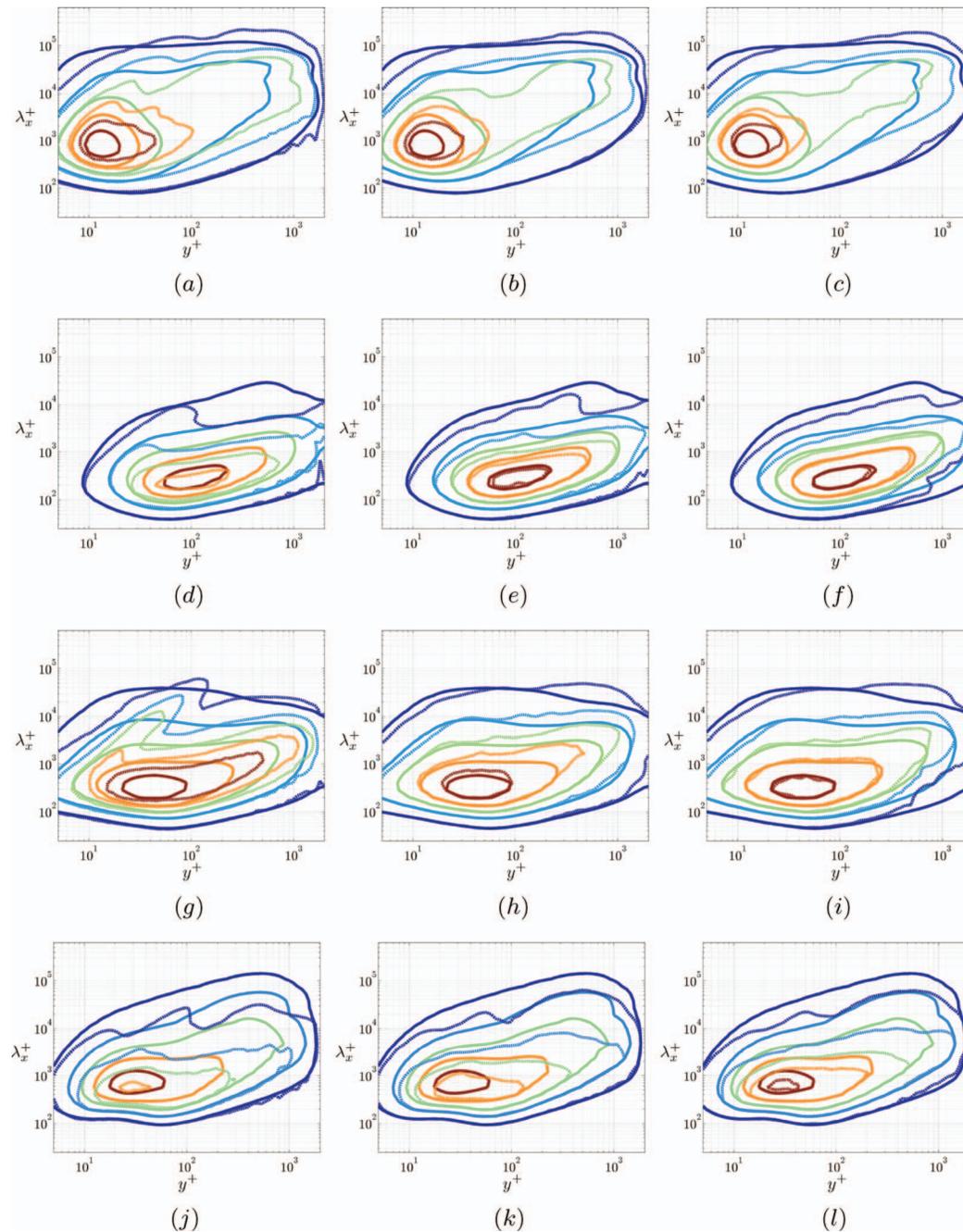
FIG. 2. The solid contours are the time-averaged spectra from DNS[11] for $Re_\tau = 2003$: (a)–(c) $E_{uu,\text{DNS}}$, (d)–(f) $E_{vv,\text{DNS}}$, (g)–(i) $E_{ww,\text{DNS}}$, and (j)–(l) $-E_{uv,\text{DNS}}$. The dashed contours are the model-based spectra with the optimal weights using (a, d, g, j) $N = 2$, (b, e, h, k) 6, and (c, f, i, l) 12 resolvent modes per κ and $0 \le c \le U_{cl}$. The contours show 10% to 90% of the maximum in the DNS data with increments of 20%.

wall-turbulence at high Reynolds numbers. We note that our approach does not capture the phase relationships between modes with different wall-parallel wavenumbers since this information is absent in the power spectra. In addition, while the computed weights represent the best fit to the spectra, they may not yield the exact solution of the velocity field. Our ongoing research is focused on determination of the weights by analyzing the nonlinear interaction of the resolvent modes.
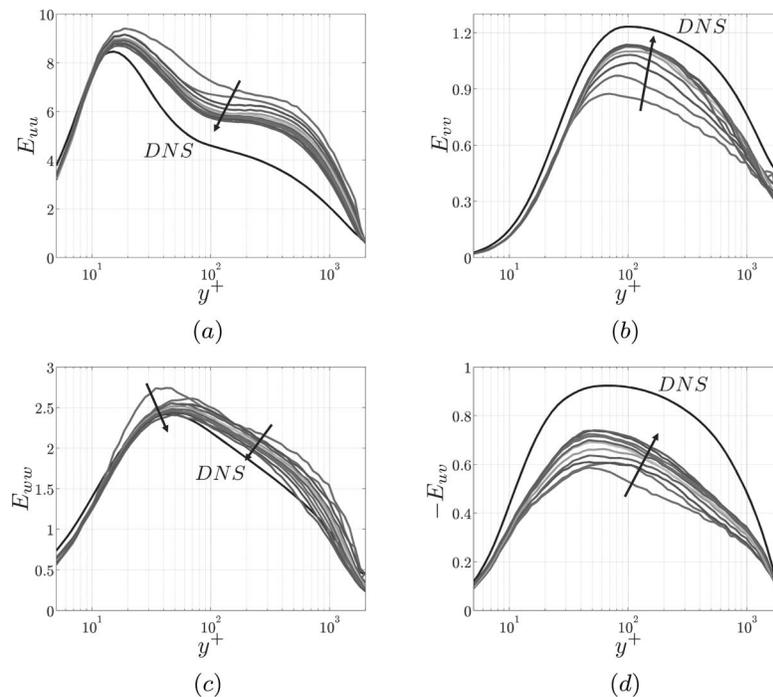
FIG. 3. The black curves are the energy intensities from DNS[11] for $Re_\tau = 2003$. The colored curves are the model-based intensities with the optimal weights using $N = 2$ to 12 resolvent modes per κ and $0 \leq c \leq U_{cl}$. Arrows show the direction of increasing N.

[1] A. J. Smits, B. J. McKeon, and I. Marusic, "High-Reynolds number wall turbulence," Annu. Rev. Fluid Mech. **43**, 353–375 (2011).

[2] G. Berkooz, P. Holmes, and J. L. Lumley, "The proper orthogonal decomposition in the analysis of turbulent flows," Annu. Rev. Fluid Mech. **25**, 539–575 (1993).

[3] C. W. Rowley, "Model reduction for fluids using balanced proper orthogonal decomposition," Int. J. Bifurcation Chaos **15**(3), 997–1013 (2005).

[4] P. J. Schmid, "Dynamic mode decomposition of numerical and experimental data," J. Fluid Mech. **656**, 5–28 (2010).

[5] A. Tumin, "The biorthogonal eigenfunction system of linear stability equations: a survey of applications to receptivity problems and to analysis of experimental and computational results," AIAA Paper 2011-3244, 2011.

[6] I. Mezić, "Analysis of fluid flows via spectral properties of the Koopman operator," Annu. Rev. Fluid Mech. **45**, 357–378 (2013).

[7] B. J. McKeon and A. S. Sharma, "A critical-layer framework for turbulent pipe flow," J. Fluid Mech. **658**, 336–382 (2010).

[8] B. J. McKeon, A. S. Sharma, and I. Jacobi, "Experimental manipulation of wall turbulence: A systems approach," Phys. Fluids **25**, 031301 (2013).

[9] A. S. Sharma and B. J. McKeon, "On coherent structure in wall turbulence," J. Fluid Mech. **728**, 196–238 (2013).

[10] R. Moarref, A. S. Sharma, J. A. Tropp, and B. J. McKeon, "Model-based scaling of the streamwise energy density in high-Reynolds number turbulent channels," J. Fluid Mech. **734**, 275–316 (2013).

[11] S. Hoyas and J. Jiménez, "Scaling of the velocity fluctuations in turbulent channels up to $Re_\tau = 2003$," Phys. Fluids **18**(1), 011702 (2006).

[12] D. E. Coles, "The law of the wake in the turbulent boundary layer," J. Fluid Mech. **1**, 191–226 (1956).

[13] J. LeHew, M. Guala, and B. J. McKeon, "A study of the three-dimensional spectral energy distribution in a zero pressure gradient turbulent boundary layer," Exp. Fluids **51**, 997–1012 (2011).

[14] R. Moarref, A. S. Sharma, J. A. Tropp, and B. J. McKeon, "On effectiveness of a rank-1 model of turbulent channels for representing the velocity spectra," AIAA Paper 2013-2480, 2013.

[15] Y. Huang and D. P. Palomar, "Rank-constrained separable semidefinite programming with applications to optimal beamforming," IEEE Trans. Signal Proces. **58**(2), 664–678 (2010).

[16] CVX Research, Inc., "CVX: Matlab Software for Disciplined Convex Programming, version 2.0 beta," see http://cvxr.com/cvx, September 2012.